Mesoscale (50–100 km) Circulations Revealed by Inverse and Classical Analysis of the JASIN Hydrographic Data

R. T. POLLARD

Institute of Oceanographic Sciences, Brook Road, Wormley, Godalming, Surrey GU8 5UB U.K.

ABSTRACT

Inverse analysis (Wunsch, 1978) has been applied to two 10-day surveys of an area 150 km square, each consisting of nearly 100 CTD stations, in order to determine the velocity field with a horizontal resolution of 45 km.

Reference levels above the main thermocline (1100 m) lead to physically implausible circulations below the thermocline. The preferred solution conserves mass with bottom velocities not significantly different from zero. All casts were repeated after 6 h, and the surveys were 20 days apart, allowing errors in the reference velocities due to internal waves, tides and changes of mass between surveys to be estimated at less than 1 cm s^{-1}.

Further spatial resolution is obtainable by classical geostrophic analysis, contouring dynamic heights with an assumed bottom level of no motion from casts 15 km apart forming triangles 45 km apart. Two regions of anticyclonic circulation are revealed, one a meander the other an eddy. The meander and eddy have different water properties, and interact as the eddy, whose diameter is 80–100 km, drifts northwestward at 2 cm s^{-1}. The circulations themselves have velocities of 10–20 cm s^{-1} and vary only weakly with depth from the surface to 1000 m, decreasing to near zero at 1500 m.

Observations from moored current meters are generally in good agreement with the geostrophic estimates, but reveal that there may be some times and places for which there is no level of no motion, sub-thermocline flows reaching 10 cm s^{-1} or more.

1. Introduction

From July to September 1978, fourteen ships and three aircraft took part in the Royal Society sponsored Joint Air-Sea Interaction experiment (JASIN, 1978) in the north Rockall Trough, northwest of Scotland (Pollard, 1978; Royal Society, 1979; Pollard et al., 1983). To provide the synoptic background for detailed study of near-surface processes, RRS *Challenger* made four hydrographic surveys of a region about 150 km square. Deduction of the velocity field from two of the *Challenger* surveys is the subject of this article.

Initially it was hoped that nine moorings covering a (300 km)^2 area (57.2–60.2°N, 8.5–13.2°W) would resolve the main circulation pattern. The velocity field they did reveal (Fig. 1) was not simple, lacking coherence between moorings 50 km apart, and changing on time scales less than a week. The only possibility of resolving smaller space scales lay in the *Challenger* data set, and led to the study reported here.

The problem is, of course, to determine reference velocities for the pairs of hydrographic stations used to calculate the geostrophic shear. The beta-spiral approach (Stommel and Schott, 1977) did not seem appropriate, as the whole hydrographic mapping area was too small (150 km) to apply beta-plane dynamics, and in any case scales less than 50 km needed to be resolved if the known variations in the velocity field were to be reasonably approximated. However, inverse analysis (Wunsch, 1978) seemed appropriate, since mass conservation should be applicable even for small volumes of ocean, and the fact that stations were repeated after 6 h would allow tidal averaging.

After describing the data (Section 2), much of the paper is devoted to the inverse analysis (Sections 3–7), estimates of errors (Section 5) and choice of reference level (Section 6). Dynamic height contours with the classical assumption of a bottom level of no motion (Section 8) provide the best possible spatial resolution, and the geostrophic velocity estimates are compared with current meter data in Section 9.

2. *Challenger* survey data

The hydrographic grid surveyed by *Challenger* is shown in Fig. 2. The 16 main grid points (referred to hereafter as A1–4, B1–4, C2–5, D2–5) were 45 km apart and round each a 15 km triangle of full-depth CTD dips was worked twice within 12 h to allow some averaging of tidal variations. Two surveys are analyzed here (Fig. 3), the B survey (31 July–9 August, days 212–221, 94 stations), and the C survey (20–30 August, days 232–242, 86 stations). All 16 main grid point triangles were occupied in the B survey, while D5 was omitted in the C survey.
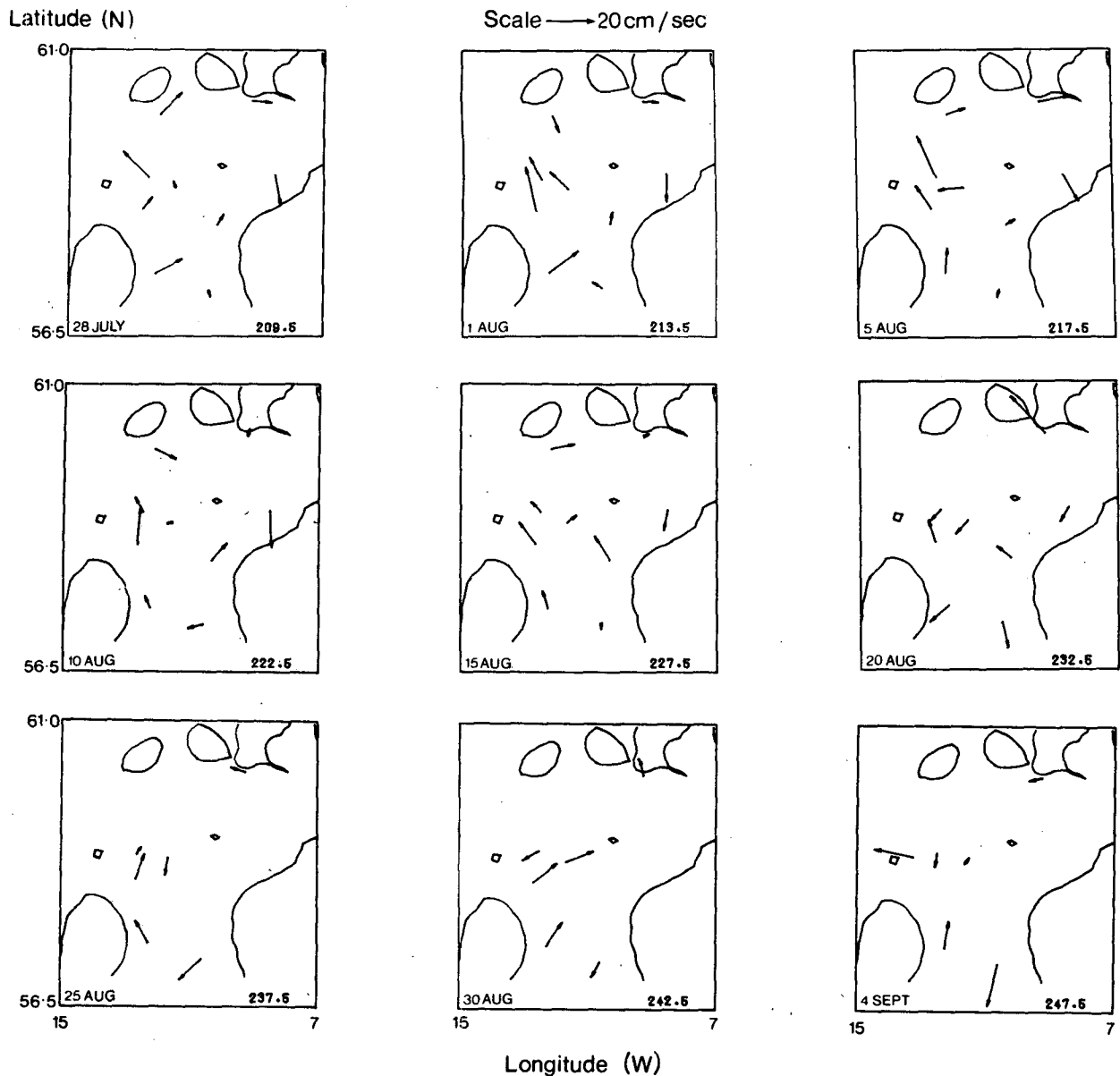
FIG. 1. After filtering to remove periodicities less than 24 hs, 1 h mean velocity vectors from instruments between 500 and 600 m on nine moorings are mapped. The maps show the low-passed values at noon at about 5-day intervals. Day of year and day/month are annotated. Arrow tails are at the geographic positions of the moorings. 500 m bottom contours are shown for comparison with Fig. 2. (From Collins and Pollard, 1982).

The individual dips were interpolated to standard pressure levels at 50 db intervals (more above 200 db) edited to remove and re-interpolate bad values of salinity and non-monotonic σ_θ values, then averaged on pressure for all dips in each triangle (normally six) to give one σ_θ profile centered at each main grid point (Fig. 4).[1]

---

[1] Note: Interpolation to standard σ_θ surfaces and then averaging the pressure values was initially attempted but abandoned because bad σ_θ values caused by bad salinities caused a high proportion of bad interpolated values. Pressure values on the other hand were error-free.

Several features of Fig. 4 are worthy of note. There is a deep layer of weak density gradient beneath the seasonal thermocline (both horizontally and vertically), extending to over 600 db, and attributable to deep winter mixing (Meincke, 1967; Ellett and Martin, 1973). The main thermocline lies between 800 and 1300 db. Salinities differ by up to 0.1‰ between profiles. The most saline water is in the south of the survey area (profile A3) but since it is also the lightest water, it is the warmest in the region, comprising North Atlantic water (Dooley and Meincke, 1981) that has flowed northward up the Rockall Trough. The freshest (coldest) water is found at triangle D5,
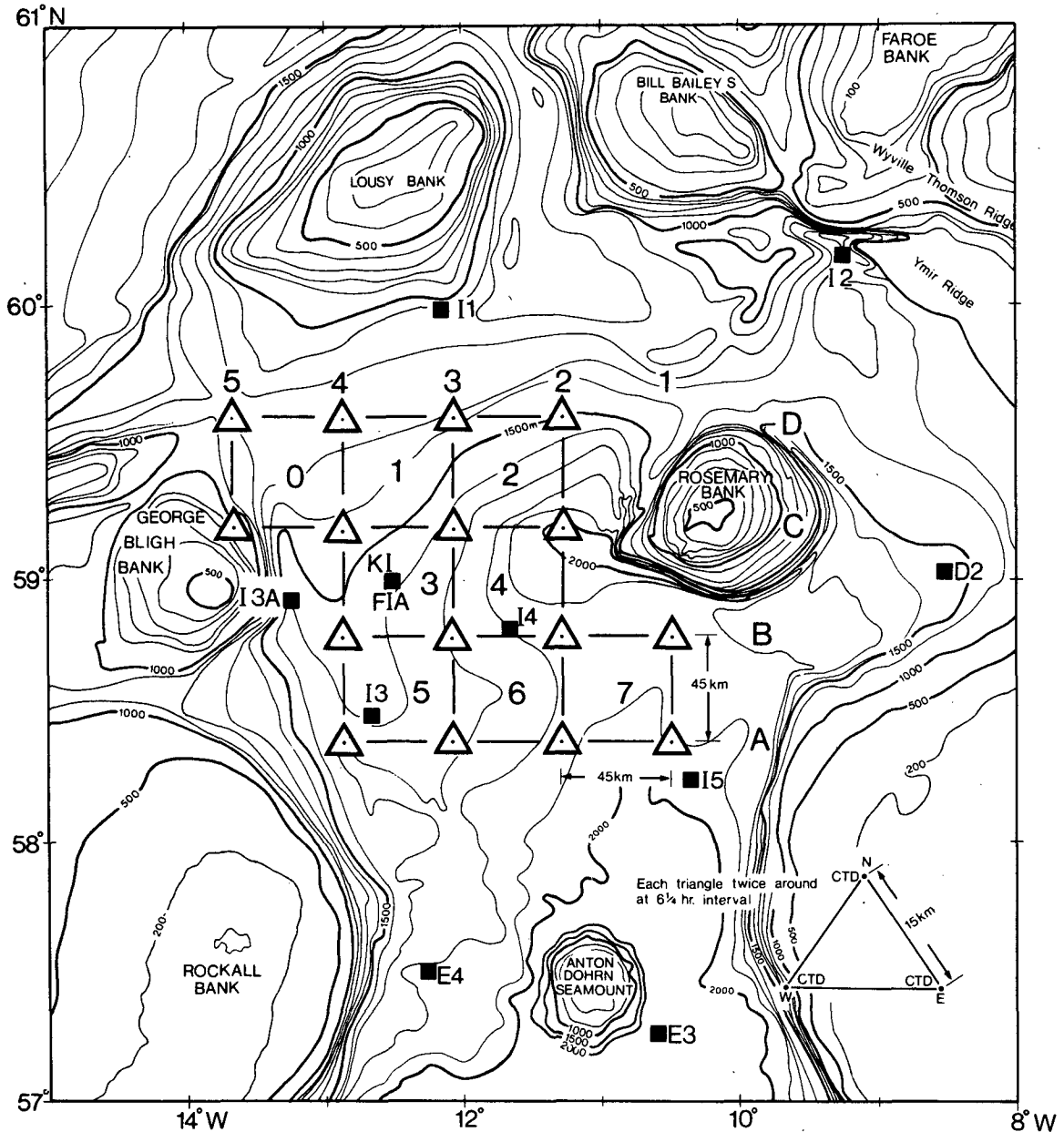
FIG. 2. JASIN 1978 hydrographic grid. There were 16 triangles in all, labeled A1 through D5. RRS *Challenger* made six casts round each triangle, as shown in the inset. Boxes used in the inverse computation are labelled 0–7. Moorings are indicated by solid squares.

the northwestern corner of the area, and has most likely originated west of George Bligh Bank (Fig. 2), outside the Rockall Trough. The range of salinities indicates that the scales of motion are smaller than the 150 km survey area.

Several salinity profiles show an increase in salinity at the bottom, caused by water from the Faroe-Shetland Channel spilling over the Wyville-Thomson Ridge (Dooley and Meincke, 1981) and spreading through the JASIN area (Ellett *et al.*, 1983). Bottom velocities associated with such a flow must be con-

sidered when selecting a reference level for geostrophic calculations.

3. Inverse analysis

Inverse analysis is used with hydrographic data as a technique for seeking reference velocities consistent with conservation of mass. The objective is to write as many independent conservation equations as possible, and solve them for the reference velocities r_i. Since there are in general fewer equations than un-
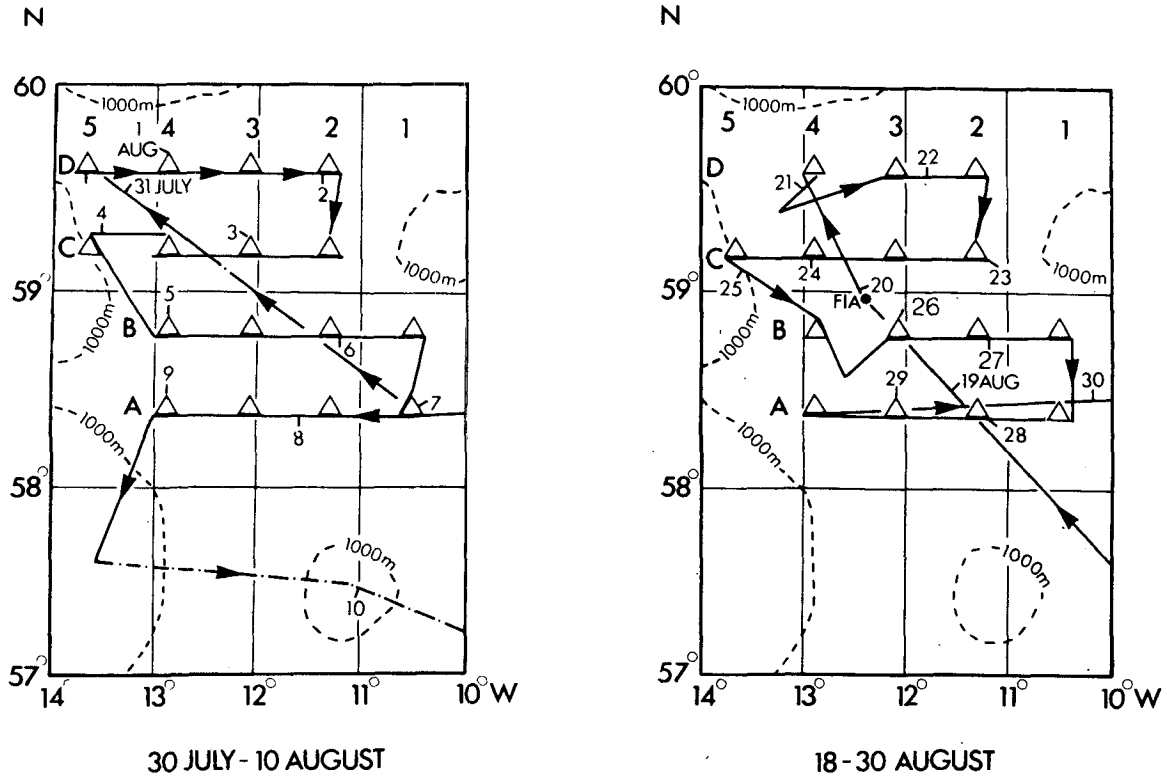
FIG. 3. RRS *Challenger* B and C hydrographic surveys (left and right, respectively). FIA refers to the Fixed Intensive Array, the focus for intensive upper ocean experiments.

known constants, the system is underdetermined, and a unique solution is achieved by minimizing the sum of squares of the reference velocities $S = \Sigma_i\, r_i^2$.

Geostrophic shears were calculated between adjacent pairs of triangle-averaged dips, and mass conservation equations constructed for seven of the 45 km square boxes shown in Fig. 2. The northwest box (box 0, Fig. 2) was omitted for most of the analysis so that the B and C surveys would be identical, but values for box 0 are included in Fig. 11.

More than one equation can be written for each box if σ_θ surfaces are used in addition to the surface and bottom to define the vertical extent of boxes. In practice it was found that two equations per box were necessary and sufficient for the following reasons:

1) The inverse technique minimizes S consistent with the constraints imposed. If there are too few constraints $S \approx 0$ and one has learned nothing. This was found to be the case with one equation per box.

2) For the seven boxes there are 20 reference velocities. Three equations per box could therefore overspecify the problem.

3) However, the shape of the density profiles (Fig. 4) makes it doubtful that three independent equations could be found for each box, in any case.

Thus two mass conservation equations were sought

for each box. Criteria applied in choosing the best equations were as follows:

1) A major problem in applying inverse techniques to the ocean is that isopycnal surfaces tend to be parallel, so ill-conditioned equations can easily result. Topography is a valuable constraint, therefore, and in the JASIN area the depth varies from 1200–2000 m (Fig. 2).

2) Interior surfaces are best chosen where there is a strong vertical density gradient to minimize errors in determining the depth from profiles.

The two equations chosen for each box, therefore, were (i) for the whole depth of water, and (ii) for water between $\sigma_\theta = 27.65$ and the bottom. The $\sigma_\theta = 27.65$ surface lies at a mean depth of 1130 db (Figs. 5 and 6) in the main thermocline (Fig. 4). Below that surface, salinities tend to be higher than those found on the Anton Dohrn section to the south (Ellett *et al.*, 1983) due to the influence of overflow water mentioned above.

Before comparing solutions with different initial assumptions, it is useful to have an estimate of the variability of a particular solution that may be caused by noisy data, incorrect assumptions and problems caused by the method of solution, such as ill condi-
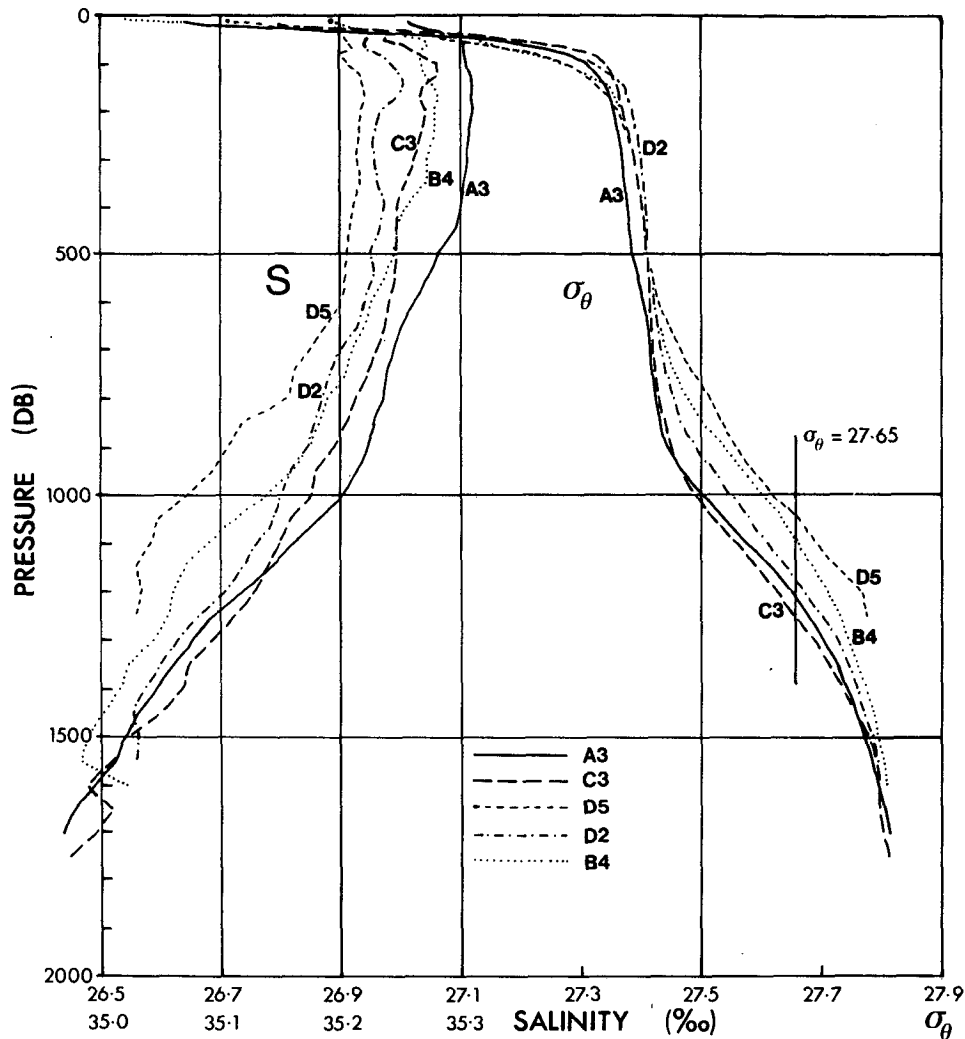
FIG. 4. Representative triangular-mean density and salinity profiles from the B survey. Most of the remaining density profiles lie between those of B4 and D2.

tioned equations. JASIN provided an exceptionally good data set for such comparisons.

4. Method of solution

We have 14 equations in the 20 unknowns r_i, in matrix notation

$$A_{(14\times20)}r_{(20\times1)} = \Gamma_{(14\times1)}, \qquad (1)$$

where r_i are the elements of the vector r. For the solution we seek (Wunsch, 1978; Lanczos, 1961, pp. 115–123), we first evaluate the eigenvalues λ_i^2 ($i = 1, 14$ with the λ_i in decreasing order) and eigenvectors $U_{i(14\times1)}$ ($i = 1, 14$) of the symmetric square matrix

$$B_{(14\times14)} = AA^T,$$

where A^T is the transpose of A. Then we obtain cor-

responding eigenvectors $V_{i(20\times1)}$ ($i = 1, 14$) by solving the shifted eigenvalue equation

$$\begin{array}{cccc} A^T & U_i & = \lambda_i & V_i \qquad (i = 1, 14), \quad (2) \\ (20\times14)(14\times1) & & (20\times1) \end{array}$$

taking the positive square roots of λ_i^2. Finally, the reference velocity vector may be written

$$r^k = \sum_{i=1}^{k} \alpha_i V_i, \qquad (3)$$

where

$$\alpha_i = \frac{1}{\lambda_i} U_i^T \Gamma. \qquad (4)$$

We also define the sum of squares

$$S^k = \sum_{i=1}^{20} (r_i^k)^2. \qquad (5)$$

The value of k depends on the rank of A. If A is of

D

1019	1119	1136	1180
x	1120	1134	1191
986 1061	1123 1135	1151 1216	1166 1148
987 1100	1117 1156	1202	1162 1148

B SURVEY

Pressures on

C

1081	1164	1259	1128
1104	1189	1263	· 1113
1118	1123 1116	1219 1234	1138 1121
1114	1120 1122	1250 1232	1164

$\sigma_\theta = 27.65$

B

1040	1139	1174	1100
1015	1146	1132	1064
1104 1102	1151 1152	1170 1129	1096 1044
1095 1128	1142 1152	1125 1144	1122 1036

A

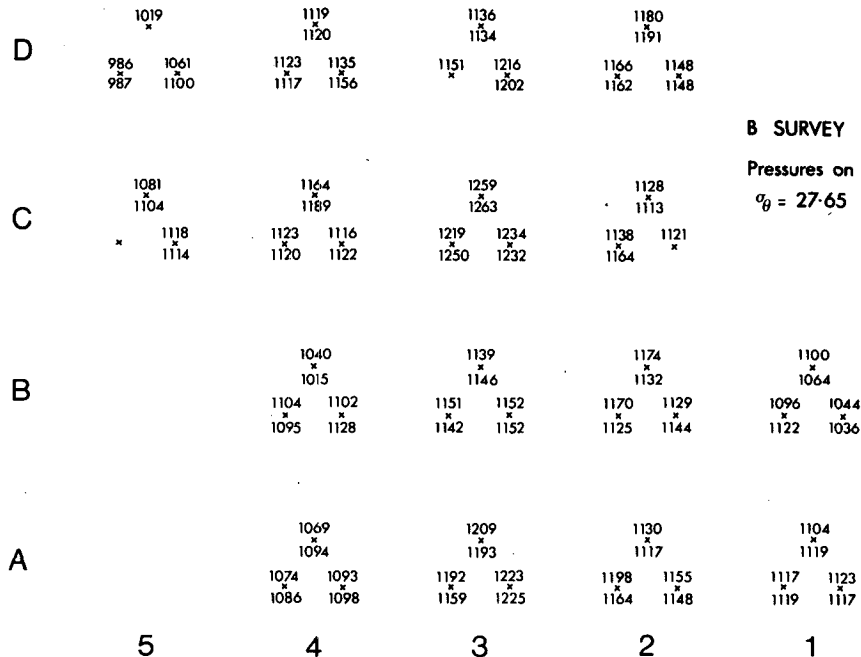| 1069 | 1209 | 1130 | 1104 |
1094	1193	1117	1119
1074 1093	1192 1223	1198 1155	1117 1123
1086 1098	1159 1225	1164 1148	1119 1117

5   4   3   2   1

FIG. 5. Pressure (db) on the $\sigma_\theta = 27.65$ isopycnal for all individual stations in the B survey. Summary statistics are shown in Table 1. An averaged contoured version of this figure is shown in Fig. 6.

full rank (14), then $k = 14$. If **A** is ill conditioned, the smallest eigenvalues (large i) will be several orders of magnitude smaller than the largest eigenvalue (λ_1). Setting $k = 14$ in this case causes the solution r to blow up as the α_i blow up for small λ_i [Eq. (4)]. In other words, the rank of **A** is less than 14, and the equations are even more underdetermined than at first sight. A solution is still obtainable (herein lies the strength and weakness of the inverse approach) by setting k equal to the rank of **A**. The weakness is that we do not know the rank of **A**, and a somewhat subjective decision is required as to how many of the smallest λ_i should be deleted. This will become apparent in the next section.

5. Error analysis

Errors in the depth of the $\sigma_\theta = 27.65$ surface arise from two sources, internal (including tidal) waves and insufficient resolution of the topography of the surface on scales < 45 km. The pressure of the 27.65 density surface for all individual stations in the B survey is shown in Fig. 5. The two casts at each station have been averaged and contoured in Fig. 6, which shows the C survey also. Summary statistics are shown in Table 1.

Tides, internal waves and positional errors for repeated stations cause pressure differences between the first and second dips at a station of 0 ± 20 db (mean $\pm$ standard deviation) for the B survey and 7 ± 29 db for the C survey. Differences between the corners of a triangle are often larger, several tens of db, with

a total pressure range of over 200 db across the survey area. Topography on the 15 km scale and above therefore dominates the noise, and the station averages are contourable with no further smoothing. For the inverse analysis, the standard deviations of the six-station triangular means are of interest, and it can be seen from Table 1b that they vary from 2 to 24 db with a mean of about 10 db.

Accordingly, gaussian random noise with zero mean and a standard deviation of 10 db was added to each 27.65 σ_θ pressure before running the inverse computation in order to examine the stability of the solution to such noise. Output from four iterations is shown in Table 2 to show the range of solutions. The example shown is for survey B, with the reference level at the bottom (specifically, at the 50 db pressure surface closest to the bottom).

To determine the rank of **A**, examine Table 2. Clearly the last eigenvalue is always too small, so the rank of **A** is no greater than 13. But it is not clear whether the rank should be taken as 11, 12 or 13. We can only say that a tendency to ill-conditioning begins to occur for $\lambda_i \lesssim 0.01 \lambda_1$. Since the sums of squares do not increase greatly from S^{11} to S^{13}, the rank is taken to be 13 hereafter.

Means and standard deviations of the 20 reference velocities from the 49 computations are shown in Fig. 7. Means range from -1.5 to 0.8 cm s^{-1} with a maximum standard deviation of under 1.0 cm s^{-1}.

When the calculation was repeated, however, it was found that the standard deviations of the means were not smaller than the standard deviations of individual
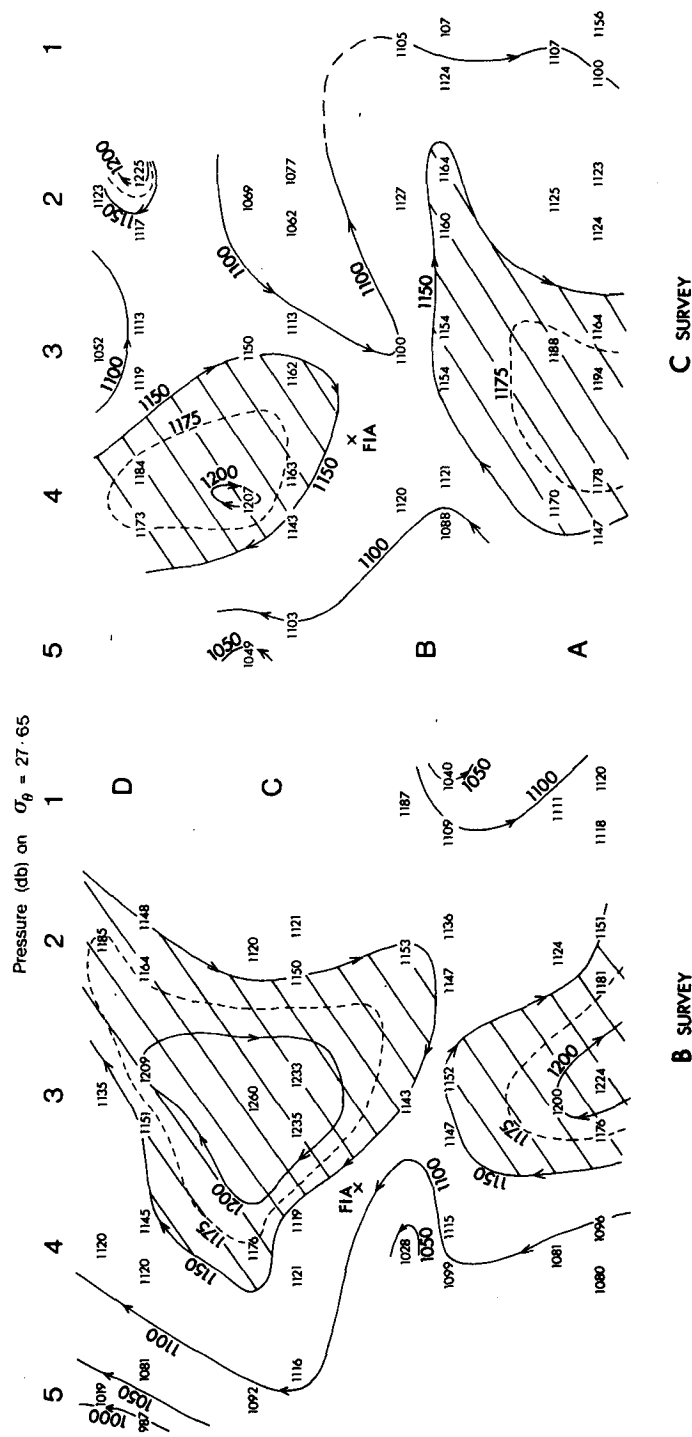
FIG. 6. Contours of two-cast averaged pressures (db) on the isopycnal surface $\sigma_\theta = 27.65$ for the B and C surveys. In both surveys the mean pressure is about 1130 db.

TABLE 1. Statistics of pressure on isopycnal surface $\sigma_\theta = 27.65$ during the B (Fig. 4) and C surveys.

(a) Pressure difference (db) between first and second dip at a point

	Number of pairs	Mean difference	Standard deviation
B survey	44	0.5	20.2
C survey	39	7.0	28.9

(b) Mean and range (db) of the standard deviations of the (usually) six-point triangular mean pressures

	Number of triangles	Mean SD	Minimum SD	Maximum SD
B survey	16	10.0	2.3	22.1
C survey	15	11.6	3.3	23.9

SD, standard deviation.

realizations, i.e., did not obey the central limit theorem. Examination of the mass conservation equations shows that the random errors in pressure affect the matrix **A**, and if **A** has a normal distribution then **r** [from Eq. (1)] has a Cauchy-like distribution (Johnson and Kotz, 1970), and the central limit theorem does not apply, as is apparent from the wide variations shown in Table 2. Nevertheless, we can conclude that variations in the reference velocities caused by internal wave noise are generally limited to about 1.0 cm s⁻¹.

The sensitivity of the inverse solution to the way in which the mass conservation equations were approximated was also tested (a) by changing the upper boundary of the lower box from $\sigma_\theta = 27.65$ to 27.75, and (b) by substituting constant extrapolation of the geostrophic velocities from the lowest level common to two profiles to the bottom for linear extrapolation. In both cases variations in the reference velocities were limited to about 1 cm s⁻¹.

Finally, the *Challenger* data set allows investigation of the effect of including a rate of change of mass term in the mass conservation equations. The term is calculated from the changes in pressure of the $27.65\sigma_\theta$ surface between surveys B and C (Fig. 6) and included in Γ [Eq. (1)]. Comparison of Figs. 9c (including rate of change of mass term) and Fig. 11d (excluding) shows no changes exceeding the 1 cm s⁻¹ variability already determined.

Of interest too is the resolution matrix (Wunsch, 1978), which measures the extent to which individual reference velocities are independently resolved. Typical sets of diagonal terms from the resolution matrix are shown in Fig. 8. A value of 1.0 signifies complete independence. For each survey, 15 out of 20 values are greater than 0.6, demonstrating rather good resolution. Note the high values surrounding box 3, the Oceanographic Intensive Area.

All non-diagonal terms in the resolution matrix (side lobes) greater than 0.3 are indicated by the solid lines. Consider, for example, resolution of velocities between D4 and C4, survey B. The diagonal term is 0.36. The off-diagonal term between D4 and D3 adds a further 0.42. All other terms add less than 0.15. It will be seen that in all cases where the diagonal term is less than 0.6, the reduction in resolution is attributable to one other station pair, usually in the same box.

6. Solutions for three reference levels

The inverse technique minimizes the sum of squares of the velocities at the reference level chosen. In one sense, this minimization can be regarded as a weakness, as it tends to support the user's choice of "level of no motion". Solutions were therefore derived for three different reference levels, 500 db, 1000 db and the bottom. Root-mean-square reference velocities and resultant rms velocities at 1500 db are summarized in Table 3 and individual 1500 db velocities are shown in Fig. 9.

Below the main thermocline, for example on the density surface $\sigma_\theta = 27.7$ (Fig. 10), salinities are higher by about 0.025‰ in the northeast of the survey area than in the south. This is the reverse of what is ob-

TABLE 2. Eigenvalues λ_i, weighting factors α_i [Eq. (4)] and sums of squares S^k (5) of the partial solutions (3) for four runs differing only in the random noise (standard deviation 10 db) added to the pressure of the $\sigma_\theta = 27.65$ density surface.

		Example 1		Example 2		Example 3		Example 4	
i	λ_i	α_i	S^i	α_i	S^i	α_i	S^i	α_i	S^i
1	4606	−0.15	0.02	−0.15	0.02	−0.14	0.02	−0.14	0.02
2	4159	0.15	0.05	0.15	0.05	0.15	0.04	0.16	0.05
3	3738	0.05	0.05	0.05	0.05	0.06	0.05	0.06	0.05
⋮	⋮								
11	82.9	−0.34	1.07	0.49	1.23	−1.74	5.00	2.17	7.80
12	56.4	1.46	3.20	1.12	2.49	2.25	10.05	−0.04	7.80
13	42.0	0.76	3.79	0.30	2.57	−0.83	10.73	−0.28	7.88
14	11.7	−6.55	46.50	−18.50	341.62	5.51	41.02	−10.81	124.53

(a) mean reference velocities (cm / sec) (b) standard deviations (cm / sec)^2

D4 0.76 D3 0.03 D2   D4 0.73 D3 0.54 D2
−0.08 −0.65 −0.14   0.24   0.46   0.15

C4 −0.95 C3 0.29 C2   C4 0.22 C3 0.13 C2
0.57   0.18   0.19   0.50   0.25   0.19

B4 −1.28 B3 −0.30 B2 −0.01 B1   B4 0.52 B3 0.33 B2 0.46 B1
−1.46   −0.61   −0.11   0.27   0.84   0.75   0.43   0.61

A4 −0.68 A3 −0.02 A2 0.24 A1   A4 0.29 A3 0.45 A2 0.64 A1

B Survey   C Survey

FIG. 7. The inverse calculation was made for the B survey, with unknown reference velocities at the bottom. The calculation was repeated 49 times, differing only in the Gaussian random noise with zero mean and 10 db standard deviation added to the pressure on $\sigma_\theta = 27.65$. The mean values (a) of the 20 reference velocities after 13 iterations (see text and Table 2) and their standard deviations (b) are shown. Positive reference velocities are north or east for east-west or north–south station pairs, respectively.

served above the thermocline (Fig. 4) and is indicative of overflow water from the Faroe-Shetland Channel (Dooley and Meincke, 1981, Ellett et al., 1983) moving westward in the vicinity of triangles C2, D2, C3, D3, C4 and D4. One might thus expect south or westward flow in the northeast of the survey area. The velocities of Figs. 9a and 9b do not fit such a picture, being implausibly large and in the wrong direction. The eastward flow between C2 and D2, for example, cannot continue to the east without rising to 1400 m north of Rosemary Bank.

Taking the bottom as a reference level yields a more plausible flow (Fig. 9c) at 1500 db, though in this case the flow is not significantly different from zero. Although we cannot rule out the possibility that there is no level of no motion, the bottom at least provides a consistent near-zero reference level from the point of view of mass conservation, and is thus taken as the reference level hereafter. Note, however, that the choice of reference level has little effect on the flows near the FIA (box 3) and along the line from B2-B3, which are all small at 1500 db.

Diagonal terms of resolution matrix

D4 0.70 D3 0.74 D2   D4 0.44 D3 0.84 D2
0.36   0.73   0.59   0.56   0.74   0.52

C4 0.86 C3 0.63 C2   C4 0.69 C3 0.68 C2
0.63   0.86   0.86   0.86   0.76   0.90   0.88

B4 0.93 B3 0.66 B2 0.31 B1   B4 0.87 B3 0.74 B2 0.63 B1
0.98   0.81   0.86   0.84   0.60   0.91   0.87   0.75

A4 0.68 A3 0.55 A2 0.46 A1   A4 0.44 A3 0.89 A2 0.33 A1

B Survey   C Survey

FIG. 8. The 20 diagonal terms of the resolution matrix (Wunsch, 1978) are plotted between the corresponding station pairs of the hydrographic grid. A value of 1.0 means the corresponding reference velocity is fully resolved by the inverse solution. Off-diagonal terms greater than 0.3 are indicated by solid lines.

TABLE 3. Root-mean-square speeds (cm s^{-1}) between hydrographic grid points.

Survey	Depth of rms speed	Reference level		
		500 db	1000 db	Bottom
B	ref. level	3.1	2.2	0.6
B	1500 db	4.0	2.4	0.7
C	ref. level	2.3	1.3	0.4
C	1500 db	2.3	1.9	0.7

7. Solutions for B and C surveys

Once solutions have been obtained with the bottom as reference level, and after 13 iterations, it is a simple matter to construct speeds across the sections at standard levels (Figs. 11 and 12). Probable water paths (by continuity) have been shaded, but it should be noted that they do not resolve the velocity field, as only speed normal to each section is resolved by the method.

The B survey (Fig. 11) reveals a complex system of eddies with anticyclonic flow around A3 and C3, cyclonic around B1, B4 and D5. In the C survey (Fig. 12) the flow is significantly different. Anticyclonic flow is still present around A3 and A4, but the only other clear feature is southward flow between D3 and D4, which turns east and exits the array between B2 and C2, possibly partly re-entering the array between B1 and B2. In both surveys shear between 50 and 500 db is weak.

Given so much structure on the scale of the station
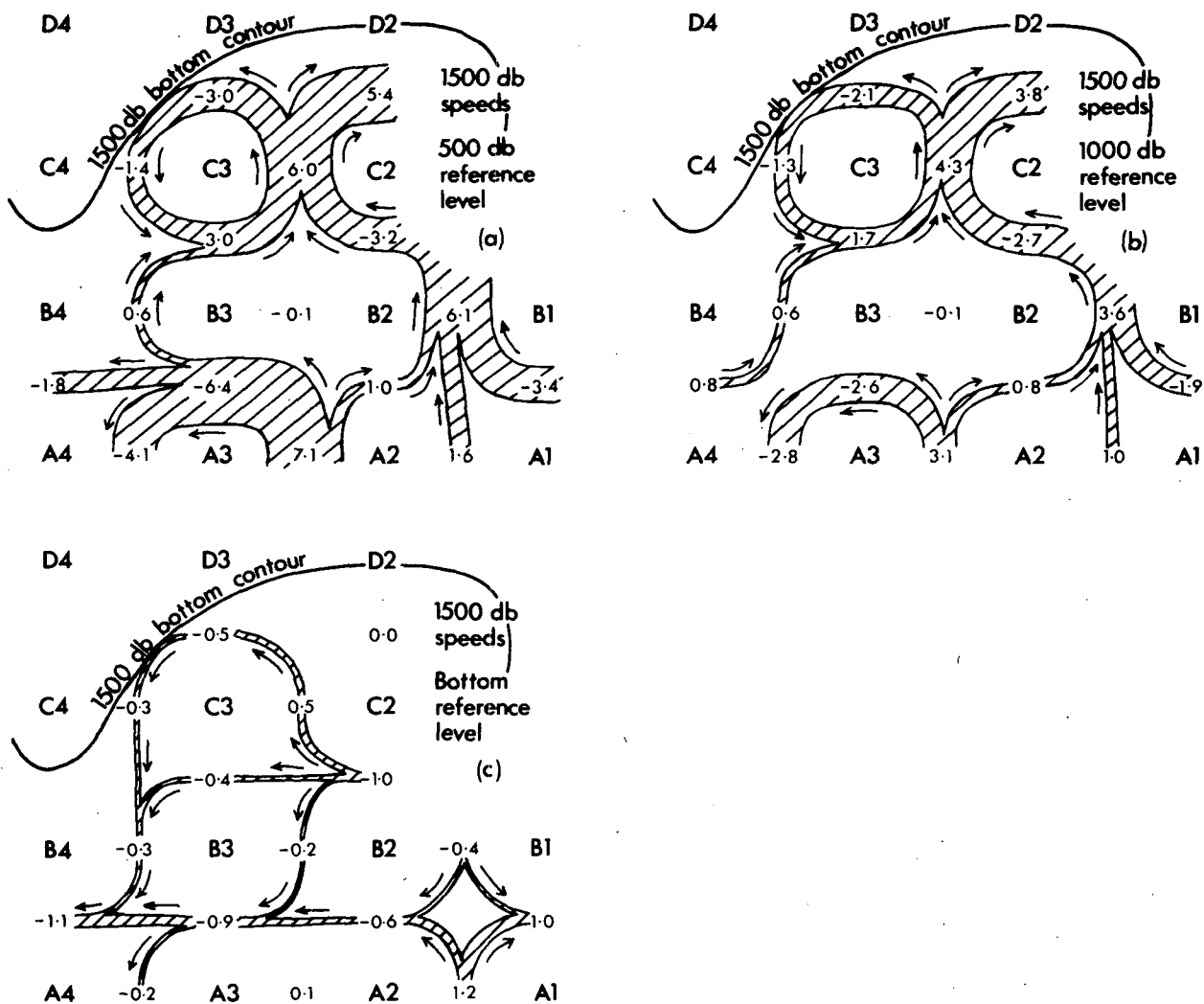
FIG. 9. Solutions for 1500 db speeds for the B survey with three choices of reference level: 500 db, 1000 db and the bottom. The 1500 db speed (cm s^{-1}) for each pair of stations is shown, being positive for east or northward values. Inferred water paths are shaded and arrowed. A term for the rate of change of mass within the lower box due to vertical motion of the 27.65 σ_θ surface (difference of Fig. 6b and 6a) has been included.

B Survey Salinity on $\sigma_\theta = 27.7$

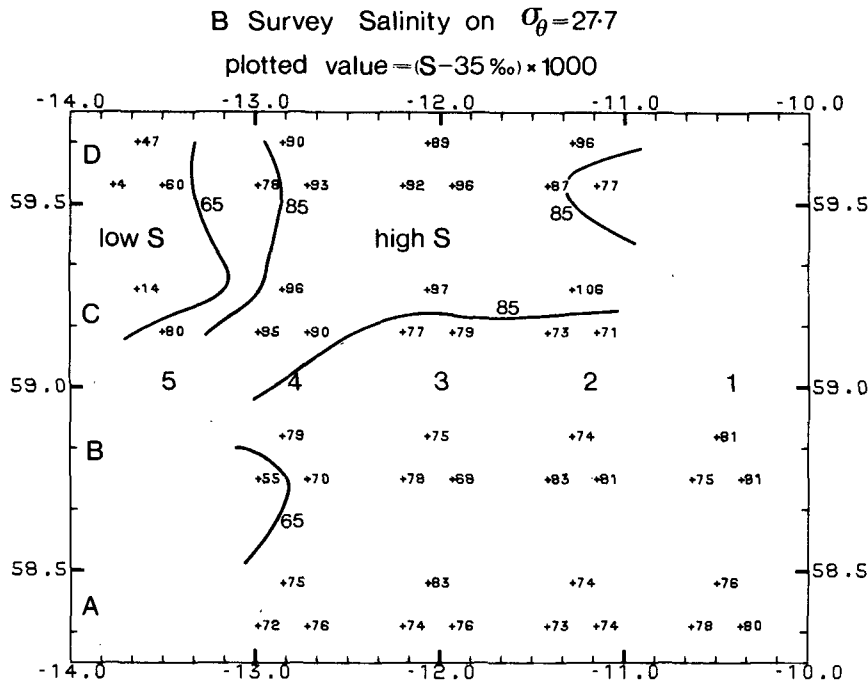plotted value $= (S - 35\text{‰}) \times 1000$

FIG. 10. Two-cast averaged salinities for the B survey on the density surface $\sigma_\theta = 27.7$ at a mean pressure of 1220 db. Salinities subdivide naturally into three ranges, separated by 35.065 and 35.085‰ as shown.

separation (45 km), one might doubt the reality of the eddies in Fig. 11. Are smaller scales aliased? Examination of Fig. 6 allays this doubt. The weak horizontal density gradients above 700 db (Fig. 4) and below 1400 db mean that geostrophic velocity shears are weak in those regions. Geostrophic velocities above 700 db are therefore dominated by the depth of the main thermocline, as shown by the contours of Fig. 6. The spatial resolution that has been gained by separating the corners of each triangle has not changed the eddy pattern. The five eddies mentioned above are still distinguishable, but it is apparent that the two anticyclonic eddies dominate the area.

It can also be seen that the anticyclonic flows are still present during the C survey. The southern one has spread to the east, and the northern one has moved to the northwest. The southward flow mentioned with reference to Fig. 12 is in fact the eastern flank of the northern eddy, and it is probable that the flow in box 3 (B3/C3/C4/B4) has been misrepresented in Fig. 12. The northward flow of 1.7 cm s^{-1} between B3 and B4 is part of the southern eddy and should turn east between B3 and C3, not west as shown. The southward flow between C3 and C4 is similarly part of the northern eddy and should exit the box between B4 and C4.

8. Classical analysis with bottom level of no motion

Contouring the depth of the main thermocline (Fig. 6) gives confidence that spatial resolution can

be improved by treating every triangle corner separately, averaging only the two stations (separated by about 6 h) at each corner. But further analysis is needed to quantify the velocities as functions of depth.

An attempt to use inverse analysis with the increased number of unknowns was abandoned as time-consuming. More fruitfully, since the inverse analysis had given confidence that it was reasonable to take the bottom as a zero reference level, dynamic heights were computed for each averaged station and then adjusted with respect to neighboring stations to force the bottom velocities to be near-zero. Specifically, the dynamic heights of the two deepest stations (2000 db) in triangle C2 (Fig. 2) were set to zero at 2000 db. Then surrounding stations that reached 1950 db were sought, and their dynamic heights at 1950 db reset to the average of those at 1950 db for the first two stations, and so on.

The level-of-no-motion hypothesis may be tested by examining the resulting dynamic height contours at 1500 db (Fig. 13). A weak anticyclonic flow is suggested for both B and C surveys with geostrophic velocities no greater than 2 cm s^{-1}. Since the velocities at 200 db are generally 5–15 cm s^{-1} (Fig. 14), the circulation above the main thermocline would be little altered if 1500 db (say) replaced the bottom as the level of no motion.

The dynamic heights in Fig. 14 have been contoured as objectively as possible by linear interpola-
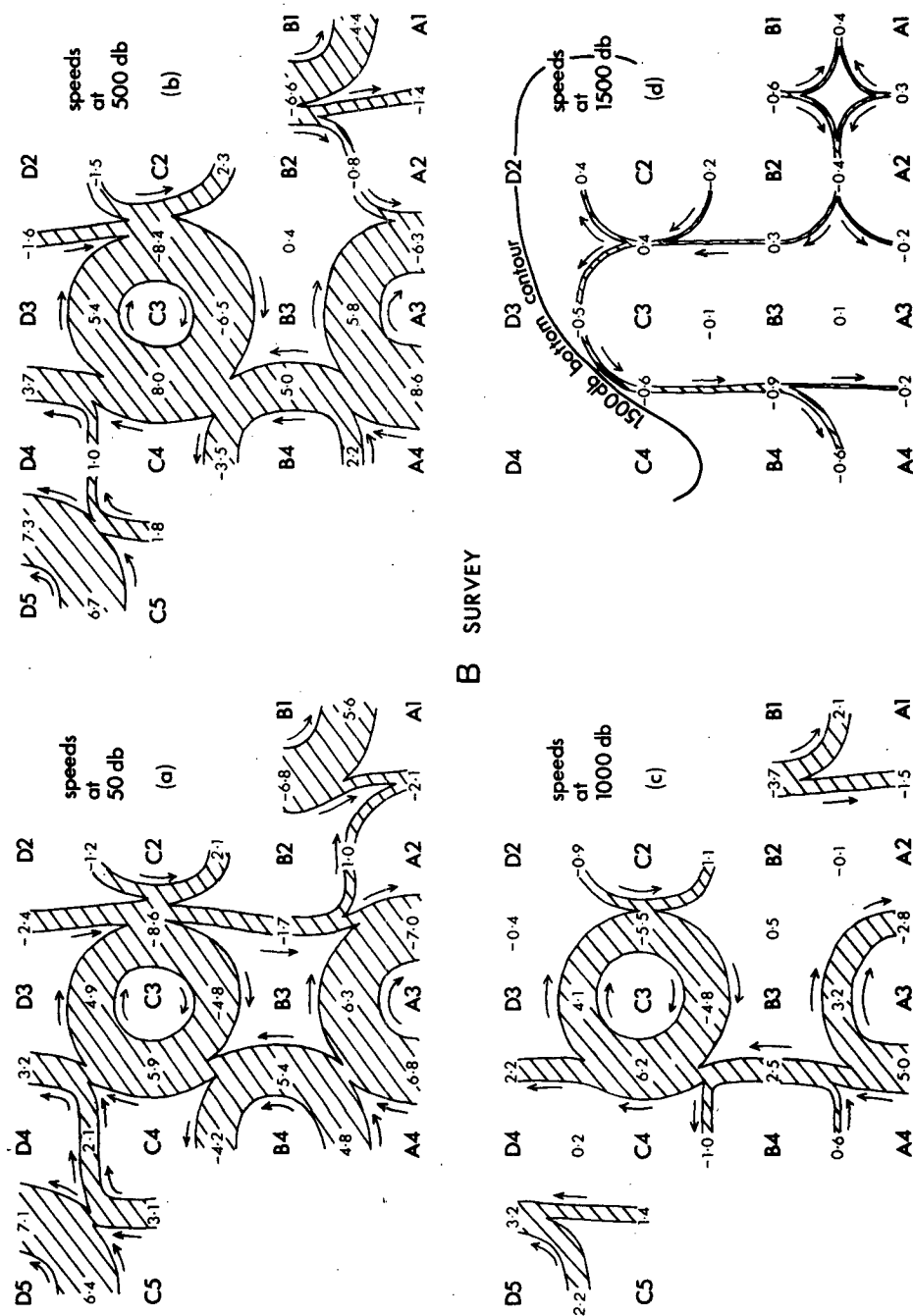
FIG. 11. Solutions for 50, 500, 1000 and 1500 db speeds for the B survey, taking the bottom as reference level. For further explanation refer to Fig. 9, but note that the rate of change of mass term has been excluded.
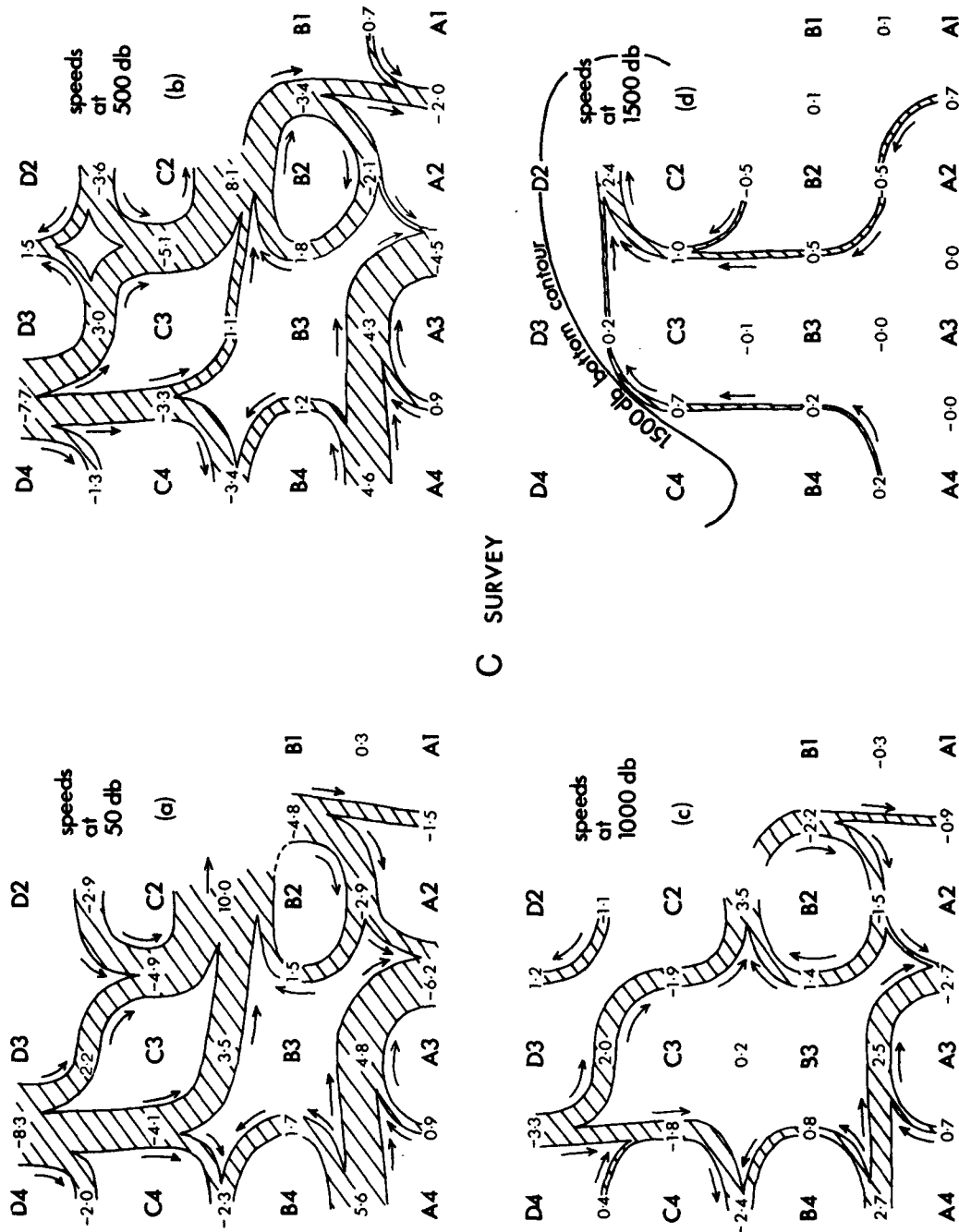
C SURVEY

FIG. 12. As in Fig. 11 but for the C survey.
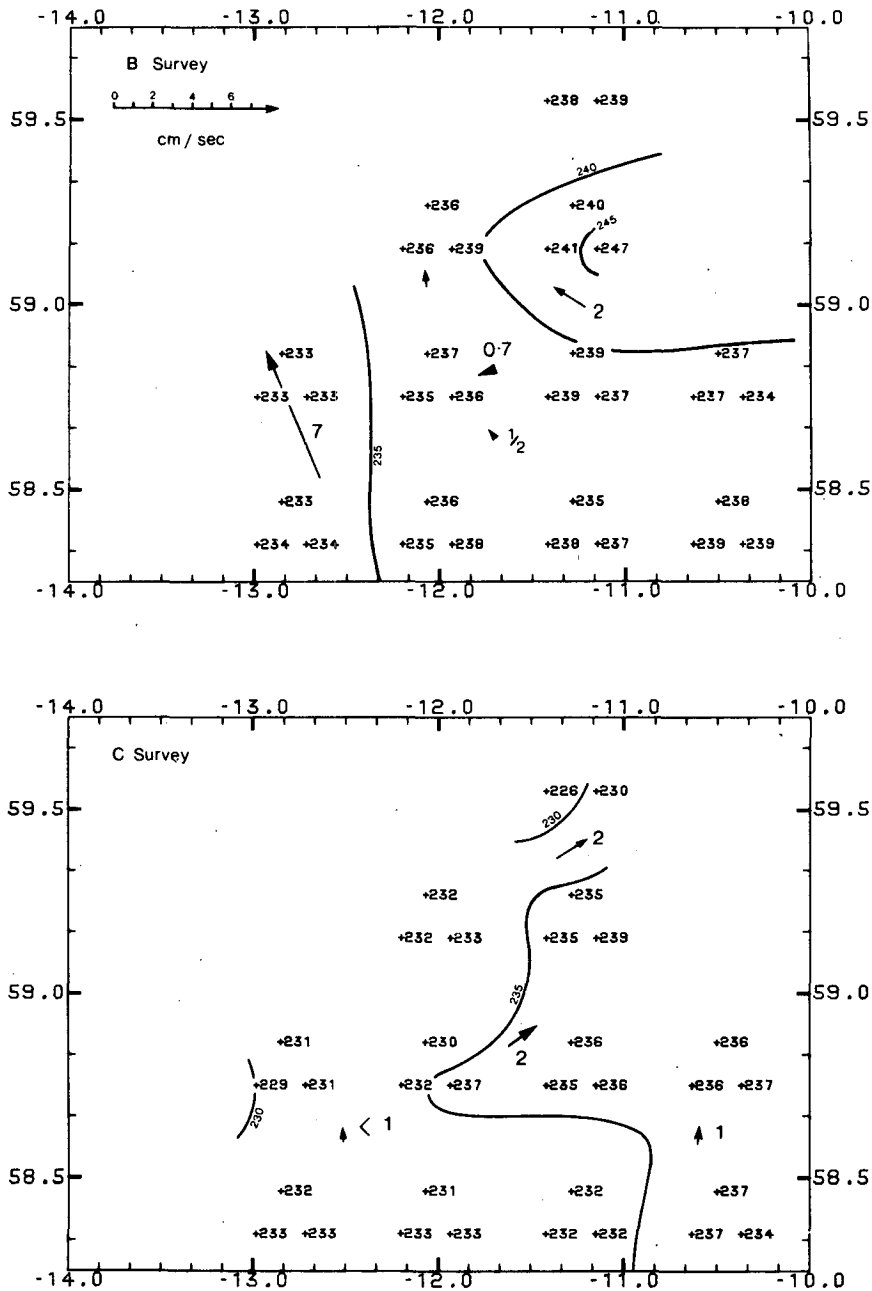
1500 db dynamic heights   (in dynamic mm)

FIG. 13. 1500 db dynamic heights (dyn mm) are shown and crudely contoured for the averaged pairs of casts at each corner of each triangle for the B and C surveys. The dynamic heights at each station have been adjusted so that the value for the 50 db level nearest to the bottom is the same as those at the corresponding depth for the nearest deeper stations, i.e., the bottom is the level of no motion. Zero dynamic height is at 2000 db for the deepest stations which are in triangle C2 (Fig. 2). A geostrophic velocity scale is given in Fig. 14. Estimated geostrophic velocities are shown with lightface arrows and observations from moored 1500 m current meters taken from Fig. 15 with boldface arrows.

tion between adjacent stations, though the contouring is unavoidably subjective near the saddle points. The anticyclonic eddy centered on C3 in the B survey is well resolved and the possibility that smaller scales are aliased (compare Fig. 11) is dispelled. The addition of triangle C5 in the C survey (cf. Figs. 14b and
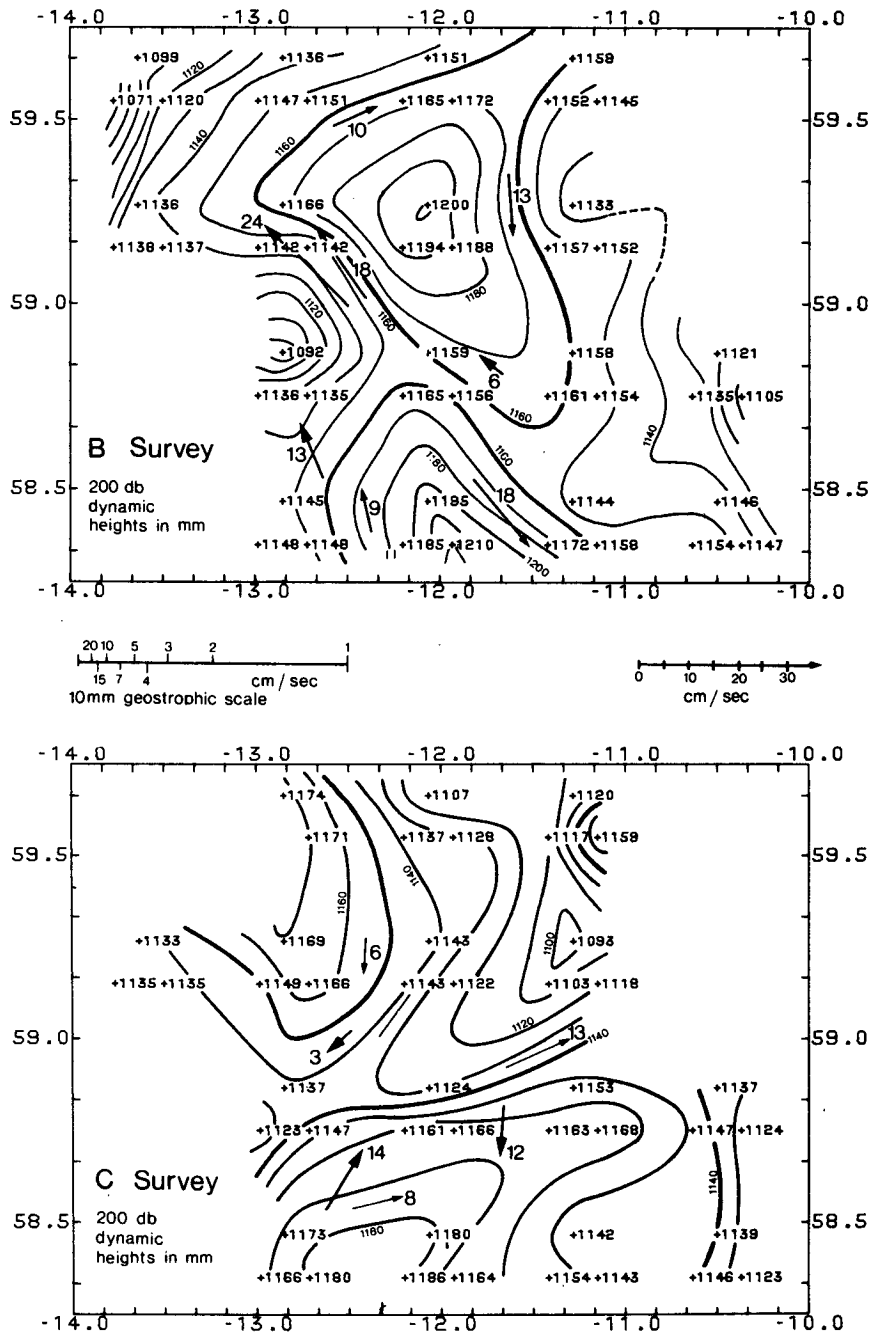
FIG. 14. 200 db dynamic heights (dyn mm) for the B and C surveys adjusted to a bottom level of no motion as described in the caption of Fig. 13. Dynamic heights are about 20 mm higher for the B survey than the C survey, ascribed to a calibration error that led to low salinities for the entire B survey. Geostrophic velocities may be inferred from the separation of 10 mm contours using the "geostrophic scale." Estimated geostrophic velocities are shown with lightface arrows and observations from moored 200 m current meters taken from Fig. 15 with boldface arrows.

Fig. 12) allows us to conclude that the eddy has moved about 60 km to the northwest between the two surveys, at an average speed of 3 cm s⁻¹.

The T/S relation in the southern region of anti-

cyclonic circulation, around A3, is the same as was found between Anton Dohrn Seamount and Rockall Bank (Ellett et al., 1983). The flow around A3 is most probably not an eddy, therefore, but a meander at

the northern extremity of North Atlantic water that has come from the south. Salinities in the meander (Fig. 4, profile A3) reach over 35.3‰. In the northern anticyclonic eddy (profile C3), salinities reach only 35.25–35.26‰ in the top few hundred metres, demonstrating that the C3 eddy has not broken off from the A3 meander. The eddy has more probably originated from the north, as suggested by the tail between D2 and D3 in the B survey (Fig. 14a). As the eddy moves west across the survey area, it interacts with the meander, causing a confluence zone along the northwest-to-southeast line C4 to B3. The resultant fronts will be described in subsequent papers.

9. Comparison with moored current meters

Estimated geostrophic velocities have been compared with current meter data from three moorings, K1, I3 and I4 (positions in Fig. 2) taken from Collins and Pollard (1982). The velocity vectors are shown in Fig. 15, and the 200 db observed velocities are also plotted on Fig. 14. In comparing the vectors, it should be borne in mind that

1) The inverse relation between dynamic height contour separation and geostrophic velocity (scale on Fig. 14) means that large geostrophic velocities are poorly resolved. The 18 cm s^{-1} geostrophic value at
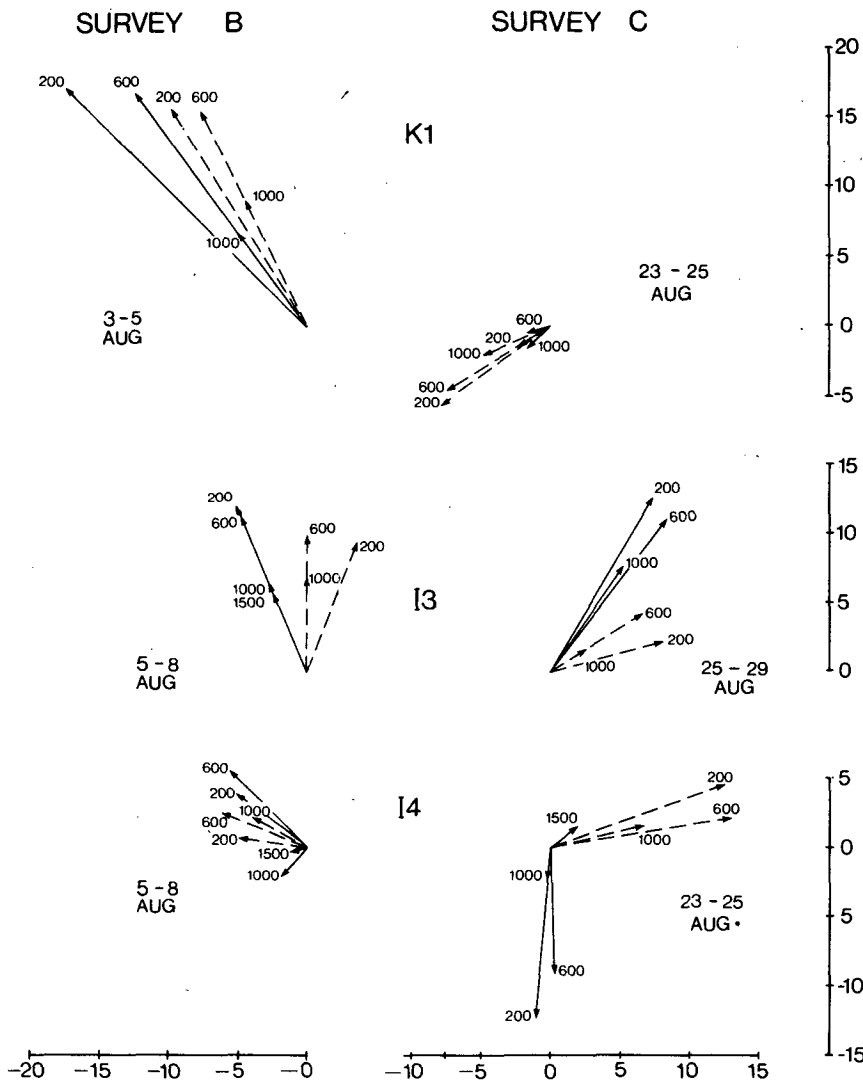

FIG. 15. Geostrophic (dashed line) and moored current meter (solid line) velocity vectors at 200, 600, 1000 and 1500 db for B and C surveys at moorings K1, I3 and I4. Geostrophic velocities have been estimated from direction and separation of dynamic height contours (e.g., Fig. 14). Observed currents are 3–4 day averages (dates on figures) covering the period during which the stations near to the mooring were worked (but see text). Observed 1500 db currents are not always available, and geostrophic 1500 db currents are all less than 1 cm s^{-1}, so have been omitted for clarity.

200 db (K1, B survey) could for example be increased to the observed 24 cm s^{-1} by minor recontouring of the nearby saddle point.

2) Three-to-five day averages of the observed flow may not match the spatial and temporal averaging of the geostrophic calculations. At I4 (200 db, B survey), for example, the observed velocity vector averaged over 5–8 August was $(-5.0, 3.8)$ cm s^{-1}. Averaged over 8–11 August, it was $(-2.5, -1.2)$ cm s^{-1}, compared to the estimated geostrophic velocity of $(-4.9, 0.7)$ cm s^{-1}.

With these provisos, the main features of Fig. 15 are as follows. At K1, the current backs from strong (20 cm s^{-1}) northwestward to weak (2 cm s^{-1}) southwestward between the B and C surveys as the eddy passes to the north. Both the backing and weakening are reflected geostrophically. At I3, the direction of the current varies very little with depth within each survey, and differs from the geostrophic directions by 25–45°. The directional discrepancy could be easily reduced by minor recontouring consistent with the hydrographic data, since the contours curve near I3 and there are saddle points or ridges on both sides of it. The fact that the observed current at 1500 db is still 7 cm s^{-1} (and was as high as 17 cm s^{-1} on 2 August) is more worrying, suggesting that there may not be a level of no motion in the meander—a useful reminder that one should not put too much faith in the results of inverse analysis.

At I4, the observed current backed during the B survey [refer to 2) two paragraphs above] consistent with being in the tail of the eddy as suggested by the contours of Fig. 14. During the C survey, the geostrophic/observed current comparison is bad, most probably because the observed currents are unrepresentative of the survey period. Mooring I4 was recovered and replaced during the survey so there are no data for 26–28 August. The average plotted is for 23–25 August, but the triangles around I4 were surveyed from 23–28 August. At 1000 db, the flow backs from south to east on the 26th, and after the mooring was replaced (29 August) flows were strong (21 cm s^{-1} at 200 m, 14 at 500 m, 8 at 1000 m) and to the northeast.

The general conclusion is that the main features of the flow with scales of, say, 30 km or more are resolved by the hydrographic survey and are consistent with observed currents. But there are also smaller structures, such as the cyclonic eddy around B4 (Fig. 14a) and the confluence zone along the line C4/B3/B2 that are not fully resolved by the hydrographic survey.

10. Summary

Eighty to ninety CTD stations covering an area of $(150 \text{ km})^2$ have been used to deduce the geostrophic velocity field by both inverse and classical methods.

With hindsight, it can be argued that the "level of no motion" could have been deduced to be near the bottom from the density profiles (Fig. 4), rendering the inverse analysis unnecessary. But the choice was not obvious a priori, and expert opinion differed. In any event, several useful conclusions can be drawn from the application of inverse methods to the Challenger data set:

1) Continuity of mass can be satisfied by choosing reference velocities of zero at the bottom (which varies between 1300 and 2000 m), with errors of no more than 1 cm s^{-1}. But 1500 m current meter records suggest that, at some positions, there were periods when velocities were non-zero throughout the water column.

2) Levels of no motion in or above the main thermocline (1000 or 500 m) do not satisfy continuity. The minimum rms reference velocities determined by the inverse method lay between 1.3 and 3.1 cm s^{-1} and led to implausible circulation patterns at 1500 db.

3) The effects of several sources of error, both observational and physical, on the inverse solution were tested. These included (a) random tidal variations in the depth of a density surface with a standard deviation of 10 db; (b) allowing for real changes in mass with time due to changes in the depth of density surfaces of up to 120 m in 20 days; and (c) constant or linear extrapolation of geostrophic velocity shear across the bottom 50 m of the profile. In all cases, variations in components of the solution vector were generally less than one cm/sec.

4) Inverse analysis, with about 13 well-conditioned equations and 20 unknowns, worked well on a near-synoptic data set collected over 10 days with station separation of 15–30 km.

5) There is some subjectivity in determining how many eigensolutions to include in the partial sum [Eq. (3)] to avoid an ill-conditioned result. In this study, solutions became unstable to small perturbations of the matrix **A** for eigenvalues smaller than about 1% of the maximum eigenvalue.

6) The 45 km boxes in which mass continuity was applied were barely small enough to resolve the flow field.

In this paper, discussion has been restricted to methods of obtaining the best velocity field from a hydrographic data set. Having found an eddy, it is of considerable interest to describe its origin, structure and dynamic behavior. Does it mix or transport heat? Does it modify air-sea interaction processes? Such topics are the subject of other papers in preparation by JASIN participants.

REFERENCES

Collins, D. S., and R. T. Pollard, 1982: Daily plots of current vectors obtained during JASIN 1978. *Internal Rep. No. 29,* Institute of Oceanographic Sciences, 144 pp.

Dooley, H. D., and J. Meincke, 1981: Circulation and water masses in the Faroese Channels during Overflow '73. *Dtsch. Hydrogr. Z.,* **34,** 41–55.

Ellett, D. J., and J. H. A. Martin, 1973: The physical and chemical oceanography of the Rockall Channel. *Deep-Sea Res.,* **20,** 585–625.

——, P. Kruseman, G. J. Prangsma, R. T. Pollard, H. van Aken, A. Edwards, H. D. Dooley and W. J. Gould, 1983: Water masses and mesoscale circulation of north Rockall Trough waters during JASIN 1978. *Phil. Trans. Roy. Soc. London,* A308, 231–252.

Johnson, N. L., and S. Kotz, 1970: *Continuous Univariate Distributions,* Vol. 1. Houghton Mifflin, 300 pp.

Lanczos, C., 1961: *Linear Differential Operators.* van Nostrand, 564 pp.

Meincke, J., 1967: Die Tiefe des jahreszeitlichen Dichteschwankungen im Nord Atlantischen Ozean, *Kieler Meeresforsch.,* **23,** 1–15.

Pollard, R. T., 1978: The Joint Air-Sea Interaction Experiment—JASIN 1978. *Bull. Amer. Meteor. Soc.,* **59,** 1310–1318.

——, T. H. Guymer and P. K. Taylor, 1983: Summary of the JASIN 1978 field experiment. *Phil. Trans. Roy. Soc. London* (in press).

Royal Society, 1979: *Air-Sea Interaction Project: Summary of the 1978 Field Experiment,* R. T. Pollard, Ed., 141 pp.

Stommel, H., and F. Schott, 1977: The beta spiral and the determination of the absolute velocity field from hydrographic station data. *Deep-Sea Res.,* **24,** 325–329.

Wunsch, C., 1978: The North Atlantic general circulation west of 50°W determined by inverse methods. *Rev. Geophys. Space Phys.,* **16,** 583–620.